

HyperRes: Efficient Hypernetwork-Based Continuous Image Restoration

Shai Aharon
Ariel University
ifryed@gmail.com

Gil Ben-Artzi
Ariel University
gilba@ariel.ac.il

Abstract

Continuous image restoration attempts to provide a model that can restore images with unseen degradation levels during training at inference time. Existing methods are limited in terms of either the accuracy of the restoration, the range of degradation levels they can support, or the size of the model they require. We introduce a novel approach that achieves the optimal accuracy of multiple dedicated models for a wide range of degradation levels with the same number of parameters as a single base model. We present a hypernetwork that can efficiently generate an image restoration network to best adapt to the required level of degradation. Experiments on popular datasets show that our approach outperforms the state-of-the-art for a variety of image restoration tasks, including denoising, DeJPEG, and super-resolution.

1. Introduction

Deep learning has demonstrated state-of-the-art results in many image restoration tasks, such as denoising [34, 35, 36] and super-resolution [20, 38, 28]. The common approach is to train the model in a supervised manner, optimizing the model for only a single degradation level. The exact degradation level of the degraded image is not known a priori, and treating all degradation levels the same lowers restoration quality. Blind image restoration [6] addresses this issue by learning to predict the specific degradation kernel for the degraded image to restore its clean version. Recently, continuous image restoration methods have gained popularity as an alternative. In these approaches, the user can adjust the restoration effect in order to generate a variety of output images and select one according to his preferences. They enable image- and user-specific adaptation for all degradation levels with a single model without the need for retraining or deploying multiple models.

Various approaches have been presented for such models [11, 32, 30, 31, 10]. State-of-the-art approaches train the network to restore two degradation levels instead of only one, an initial and final one that spans the required range of

degradation levels. At inference time, an input parameter is used to adjust the model’s weights to an unseen degradation level. In practice, however, accuracy declines as one moves from the trained to the untrained level. As a result, several models need to be trained in order to achieve accuracy across the entire range.

We present a single model that is equivalent to multiple independent models. Our model can accurately restore a wide range of degradation levels, both inside and outside the trained range, without any additional increase in its size or a decrease in its accuracy. Furthermore, deployment for any degradation level is highly efficient, requiring only a single scalar multiplication.

To this end, we introduce a hypernetwork that learns to generate the filter weights of an image restoration network conditionally based on the required restoration level, given as an input parameter. To ensure an efficient representation at inference time, we constrain the kernels corresponding to the different levels to be identical up to a scaling factor and learn only the weights’ basis vectors. In order to achieve the desired accuracy and continuity over any predefined range we train our model to generate multiple restoration networks simultaneously; each is optimized to a different degradation level. During inference, it can be easily used to efficiently generate the required filter weights on-the-fly. Fig. 1 shows the result of our approach and AdaFM [11] for super-resolution. Using our approach, we can adjust the model to achieve higher accuracy by scalar multiplication.

Contribution. We introduce a hypernetwork model for continuous image restoration tasks, which can accommodate a wide range of degradation levels, and unlike previous approaches does not sacrifice size or accuracy. It is practically as accurate as multiple dedicated models, regardless of the range of degradation levels supported. It has the same footprint as a single restoration network model and requires no additional parameters. It outperforms existing state-of-the-art models in both accuracy and size and can be easily deployed to generate at runtime state-of-the-art image restoration networks.



Figure 1: Our model achieves **higher restoration accuracy** with the size of only **a single base model** without any increase in the number of parameters, compared to AdaFM [11].

2. Related Work

Modulating Networks. Recently, there has been a growing interest in constructing networks that can be continuously tuned at inference time. These can broadly be categorized into two categories, models which allow tuning different objectives at inference time and models which allow different restoration levels of the same objective, where our approach falls into the latter category. The typical approach is to train two related networks on different objectives and apply interpolation between their weights. The networks can be either the same or with additional tuning blocks. Dynamic-Net [30] adds specialized blocks directly after the convolution layers, which are optimized during the training for the additional objective. CFSNet [31] used branches, each based on a different objective. AdaFM [11] added modulation filters after each convolution layer. DNI [32] train the same network architecture on different objective and interpolates all the parameters. Son [19] extended the approach of [11] with an FTN module allowing better non-linear interpolation. [14] generates kernels for the super-resolution task. They employ an off-the-shelf SR network [37] as a backbone which is $\times 10$ bigger than our network, and their proposed solution is applicable only for the super-resolution task. [16] proposed solving the image restoration task as a multi-task problem. Their network, however, is specialized for restoring only a limited number of degradation levels, each of which must be trained individually. In our approach, the model is trained on a small set of degradation levels and can continuously restore any other level inside and even outside this range.

Weight-generating network. Learning to learn, or meta learner, uses meta networks to generate weights for the main network for various tasks [27, 21, 17]. Hypernetwork, introduced in [9], uses a small network with a reduced number of parameters to generate the weights for a larger target network. It often uses weight sharing across layers, while reaching accurate results. [4] applied hypernetwork to Neu-

ral Architecture Search (NAS) [24, 7] aimed to create or improve the search of the whole network architecture. It was also used in Bayesian context [18], and Stochastic maximum likelihood optimization [25]. [8] presented an image restoration hypernetwork with a single main network. In our approach, we employ a hypernetwork to generate the weights of kernels in multiple target networks, such that they are linearly dependent.

3. Method

3.1. Problem Formulation

Our model consists of a hypernetwork h and main restoration networks n_i . The weights of our hypernetwork θ^h are learned during the training process and fixed during inference time. The input to hypernetwork h is a degradation level $c_i \in \mathbb{R}$ and the output is θ^{n_i} , the kernels' weights for the main restoration networks n_i , $\theta^{n_i} = h(c_i, \theta^h)$. The input for each main network n_i is a degraded image $\mathbf{I}^{c_i} \in \mathbb{R}^{3 \times H \times W}$ with a degradation level c_i , H, W are the height and width of the image and the output is the restored image with the same dimensions, $n_i(\mathbf{I}^{c_i}; \theta^{n_i})$. Given \mathbf{I}^{c_i}, c_i , the goal is to generate the weights of the corresponding restoration network n_i to optimally restore the degraded image. We achieve this goal by training the hypernetwork, h , to learn to simultaneously generate multiple main networks, each of which corresponds to a different degradation level. By jointly optimizing for multiple restoration networks, our hypernetwork learns to generate the weights for all the degradation levels across the continuous range, including unseen ones. The optimization problem associated with our model is formulated as:

$$\operatorname{argmin}_{\theta^h} \sum_{i=1}^k \mathbb{E}_{\mathbf{I}^{c_i}, \mathbf{I}} [\mathcal{L}(n_i(\mathbf{I}^{c_i}; h(c_i; \theta^h)), \mathbf{I})], \quad (1)$$

where k is the number of main networks, $\mathcal{L} : \mathbb{R}^{3 \times H \times W} \times \mathbb{R}^{3 \times H \times W} \rightarrow \mathbb{R}_+ \cup \{0\}$ is our restoration loss for the main network.

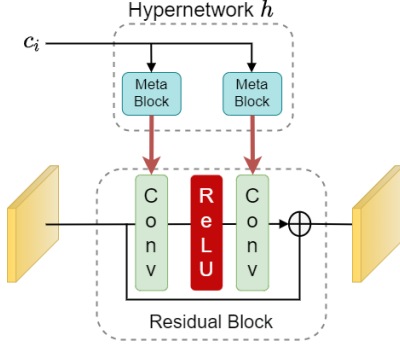


Figure 2: Our hypernetwork consists of l meta blocks, one for each convolutional layer. Each meta block is a Fully Connected (FC) layer that outputs the kernels’ weights for the corresponding kernel in the main network.

3.2. The Network

Parametrization of Main Network. The hypernetwork h consists of l meta blocks, where l is the number of kernels in the main network’s residual blocks. Each meta block is a fully connected layer constructed out of weights and biases, $\mathbf{w}^j, \mathbf{b}^j \in \mathbb{R}^{(C_{out} \times C_{in} \times K \times K) \times 1}$, where C_{in} and C_{out} are the number of input and output channels, respectively, and $K \times K$ is the kernel’s size. The j^{th} kernel of main network n_i is \mathbf{k}_i^j , of the same dimensions as the meta block. The parameters of the hypernetwork and each main network are $\theta^h = \{(\mathbf{w}^j, \mathbf{b}^j)\}_{j=1}^l, \theta^{n_i} = \{(\mathbf{k}_i^j)\}_{j=1}^l$.

We parameterize the kernels of the main network as a linear combination of our hypernetwork’s weights and biases with the degradation level as a scaling parameter. Thus, our hypernetwork h generates the weights of the j^{th} kernel of main network n_i for degradation level c_i by:

$$\mathbf{k}_i^j = c_i \mathbf{w}^j + \mathbf{b}^j. \quad (2)$$

This allows a highly efficient representation as we only need to store the weights and biases of the hypernetwork in order to generate the corresponding kernels for each possible restoration network given the degradation level. We demonstrate that, despite the compact representation, our model is highly accurate. Note that, unlike hypernetworks [9], our method assigns each meta block to generate weights for a specific main network layer with one common input scalar. Due to the bias term, the output convolutional kernels are not identical throughout the various main networks up to the input scalar. Figure 2 presents the generation of the main network’s kernels by the meta blocks.

Training. During training, the hypernetwork generates multiple main networks, each main network n_i is optimized to restore a degraded image with a corresponding degradation level c_i . The number of main networks (k) is fixed

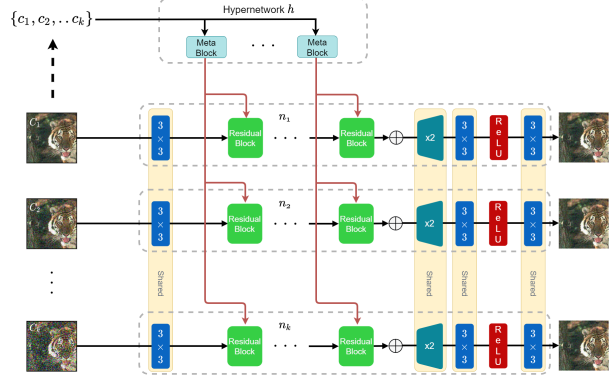


Figure 3: The training framework. Each main network is generated by the hypernetwork using the same kernels. It is fed with a corresponding degraded image, and the losses are summed and back-propagated to the shared and hypernetwork weights.

during the training process. The main network is a standard image restoration network [5]. It consists of a downsampling layer using convolution with a stride of 2, 16 residual [12] blocks and upsampling layers using pixelshuffle [29] and a skip-connection over the residual blocks. The weights of each main network are the weights of the residual block’s kernels generated by the hypernetwork (Fig. 3, green background) and the weights of the head and tail of the network which are shared among all the main networks (Fig. 3, yellow background).

Each image in the training set $\mathcal{D} = \{\mathbf{I}_1, \mathbf{I}_2, \dots, \mathbf{I}_n\}$ is degraded with k degradation levels $\{c_1, c_2, \dots, c_k\}$ and fed into the corresponding main network $\{n_1, n_2, \dots, n_k\}$. Each main network is generated according to the degradation level c_i and meta blocks. Our goal is to optimize the overall restoration accuracy under the different degradation levels. Therefore, no degradation level is privileged and our total loss is the unweighted sum of individual \mathcal{L}_1 losses. Since the aforementioned weight generation operations are completely differentiable, the parameters in our hypernetwork h are optimized simultaneously following the chain rule. The training process is illustrated in Fig. 3.

Inference. Given a degraded image and an input degradation level c_i , we employ the learned weights of the hypernetwork θ^h to generate the weights of a restoration network θ^{n_i} . Each meta block generates the weights according to Eq. 2. A simple user interface enables the user to interact with the system in real-time, selecting the input value and, as a result, the desired restoration outcome. The restoration network generation is efficient involving the multiplication of the same single scalar for all the residual block’s kernels of the main network.

4. Experiments

4.1. Implementation Details

The DIV2K[1] dataset was used to train the models for denoising, Deblocking JPEG (DeJPEG) and super-resolution. It includes 1000 2K resolution RGB images, with 800 images used for training, 100 for validation and 100 for testing. The training data is augmented by standard practice, with both horizontal flipping and rotations. The mini-batch size is set to 16. We use randomly cropped 96×96 patches from each image as our training data. The $L1$ loss[39] is used throughout all the experiments. We heuristically set the weight of each main network’s loss uniformly. We use an initial learning rate set to 1×10^{-4} , decaying by a factor of 10 after 5×10^5 iterations. We train our model for 1×10^6 iterations in total. The Adam [11] optimizer is deployed with $\beta_1 = 0.9, \beta_2 = 0.999$. We implement our approach using the PyTorch [23] library. The model is trained on an NVIDIA RTX 2080Ti GPU for approximately 12 hours.

The input degradation level for the hypernetwork is normalized by 255 for all tasks, demonstrating the robustness of our model. For denoising, we train a model with four main networks to restore noise levels $\sigma = 15, 35, 50, 75$. The input for each main network is a ground truth patch degraded by the corresponding Gaussian noise level. The output of each main network is evaluated with respect to the same ground truth input patch. For DeJPEG, we train our model with five main networks to restore compression qualities $q = 10, 25, 45, 65, 80$ using OpenCV [3] JPEG encoder, where 80 has minor artifacts, and 10 has severe high-frequency loss resulting in noticeable artifacts. Similar to [11, 32], we use grayscale images for training and testing. For super-resolution, we down-scaled images by various factors and upscaled them to the original size using OpenCV bicubic interpolation (Pre-Upscaling SR [33]). We train our model with four main networks to restore upscaling factors of $\times 2, \times 3, \times 4, \times 5$.

4.2. Restoration Quality

We evaluate our approach for the following tasks - denoising, DeJPEG and super-resolution (Fig. 1), using popular benchmarks. For denoising, we use the CBSD68 dataset [22], for DeJPEG the LIVE1 [26] and for super-resolution Set5 [2]. In all tasks, the baselines are independently trained restoration models specifically optimized to restore a single degradation level. To compare our accuracy with respect to a single continuous model (same as ours), we also include state-of-the-art models, AdaFM [11], DNI [32] and CFS-Net [31]. For denoising, they were trained on $\sigma = 15, 75$. For DeJPEG, they were trained on $q = 10, 80$. For super-resolution, they were trained on $\times 2, \times 4$. In addition, we also compare with respect to Decouple learning [8], trained

on the same objectives as ours. For each task, we report standard metrics - PSNR and SSIM [13]. In all tables bold represents the best results. For super-resolution, as commonly done, we train our model based on RGB images and evaluate the PSNR based on the y-channel. During the evaluation, our trained hypernetwork generates the weights of a *single* main network corresponding to the input degradation level, which is then used to restore the images.

For denoising, we evaluate our model with respect to all noise levels from 5 to 90 with intervals of 5. Both AdaFM and DNI share the same network structure as our standard image restoration network, with 16 residual blocks whereas Decouple learning consists of 20 blocks. Table 1 shows our main results for the denoising task, with restoration accuracy measured by PSNR and SSIM. Our technique outperforms all other methods in almost all noise levels tested, and it achieves restoration accuracy equivalent to that of dedicated models, identically in most of the range. The average PSNR distance from the optimal accuracy is negligible, 0.009. Interestingly, even when applying our model to the high noise level range of 75 – 90, our model exhibits high accuracy with an average PSNR distance of 0.006. For the lower range of noise levels, our model obtains an average PSNR distance of 0.325. To obtain a lower PSNR distance, it is possible to extend the training of our model for additional degradation levels, as discussed in the next section.

For super-resolution, we evaluate our model on five upscaling factors, $\times 2, \times 3, \times 4, \times 5, \times 6$. As before, baselines consist of multiple independent models trained to restore a particular degradation level. Table 2 shows our results. Similar to denoising, our method outperforms all other methods, with a significant PSNR difference from the second-best method.

For DeJPEG, we evaluate our model on eight different compression levels. Table 3 shows our results with respect to optimal accuracy obtained by training independent models to restore each compression level, AdaFM, DNI, CFS-Net and Decouple learning. Our approach achieves comparable PSNR accuracy to the optimal ones at all compression levels. It also achieves the highest SSIM for all compression levels. Fig. 10 shows how our methods performed on various compressed images.

4.3. Robustness

Trained Range. Our approach provides the flexibility to train the same model for different ranges of degradation levels without increasing its size at training time or compromising its accuracy at inference time. We train our model using the same amount of parameters for ten ranges of degradation levels. The model includes four main networks which are distributed uniformly across the range. Despite the increased range, all models achieve $\geq 99\%$ accuracy compared to the optimal PSNR obtained by training

Table 1: Results for image denoising. The top table is PSNR and the bottom table is SSIM. Baselines are individual models trained to restore a specific noise level. For most noise levels in the range, our approach achieves comparable accuracy to individual models, allowing accurate and fast restoration at inference time of a wide range of degradation levels with the number of parameters of only a single model.

	PSNR (dB)								
	5	15	25	35	45	55	65	75	85
Baseline	40.48	34.08	31.42	29.80	28.64	27.78	27.06	26.46	25.95
DNI	23.64	34.07	25.44	22.26	21.41	22.08	24.24	26.46	23.01
AdaFM	38.80	34.08	31.19	29.30	28.42	27.40	26.89	26.34	25.61
DeCoupling	34.40	30.87	27.65	25.46	23.89	22.74	21.87	21.22	20.72
CFSnet	29.43	29.27	28.91	28.38	27.78	27.16	26.58	26.03	25.55
Ours	39.96	34.02	31.41	29.80	28.64	27.78	27.06	26.46	25.95
Distance (Ours)	0.52	0.06	0.01	0.01	0.00	0.00	0.00	0.00	0.00

	SSIM								
	5	15	25	35	45	55	65	75	85
Baseline	0.98	0.93	0.89	0.85	0.81	0.78	0.76	0.74	0.71
DNI	0.95	0.95	0.87	0.81	0.77	0.76	0.75	0.73	0.71
AdaFM	0.97	0.95	0.88	0.84	0.80	0.77	0.75	0.73	0.70
DeCoupling	0.97	0.89	0.78	0.69	0.61	0.55	0.51	0.47	0.45
CFSNet	0.84	0.83	0.82	0.81	0.78	0.76	0.73	0.71	0.68
Ours	0.98	0.95	0.89	0.85	0.81	0.78	0.76	0.73	0.71

Table 2: Results for super-resolution task.

	PSNR (dB)					
	2	3	4	5	6	
Baseline	36.95	29.86	29.54	25.67	25.06	
DNI	24.14	23.08	23.06	21.63	21.34	
AdaFM	36.95	28.85	27.87	25.15	24.38	
DeCoupling	29.97	26.35	25.90	23.45	22.76	
CFSNet	30.47	26.29	25.40	22.90	22.30	
Ours	36.69	29.77	29.46	25.63	24.92	

	SSIM (dB)					
	2	3	4	5	6	
Baseline	0.94	0.84	0.84	0.74	0.71	
DNI	0.74	0.79	0.76	0.68	0.65	
AdaFM	0.94	0.83	0.81	0.57	0.53	
DeCoupling	0.92	0.83	0.81	0.72	0.68	
CFSNet	0.92	0.82	0.78	0.69	0.65	
Ours	0.94	0.84	0.83	0.74	0.71	

Table 3: Results for DeJPEG artifacts removal task.

	PSNR (dB)				
	10	30	50	70	80
Baseline	28.82	32.57	34.40	36.40	38.14
DNI	28.76	21.98	18.84	23.39	38.16
AdaFM	27.15	31.28	33.59	36.22	38.14
DeCoupling	28.25	31.68	33.28	35.04	36.44
CFSNet	27.63	32.12	33.72	34.88	35.48
Ours	28.81	32.56	34.39	36.38	38.09

	SSIM (dB)				
	10	30	50	70	80
Baseline	0.82	0.91	0.94	0.96	0.97
DNI	0.82	0.86	0.87	0.94	0.97
AdaFM	0.77	0.86	0.87	0.89	0.90
DeCoupling	0.81	0.91	0.93	0.95	0.96
CFSNet	0.80	0.92	0.94	0.95	0.96
Ours	0.82	0.91	0.94	0.96	0.97

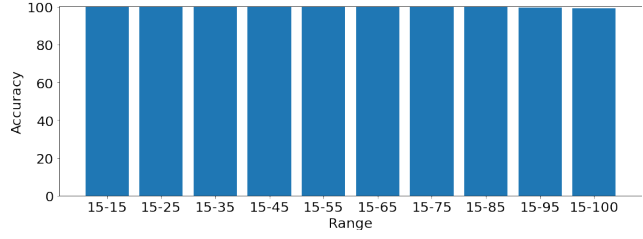


Figure 4: The x-axis is the trained range and the y-axis is the accuracy.

multiple dedicated models. The results are shown in fig. 4.

Untrained Range. Despite the fact that our approach can be trained for various ranges, the actual input degradation level might be outside the expected range in some cases. Such a case is challenging since the magnitudes of the weights can be either too high or too low than during the optimization process. Table 4 shows a comparison between our approach and existing methods for denoising. We train the same models as before for noise levels of $\sigma = 15, 75$ and evaluate them for noise levels outside that range. Our approach outperforms all other methods. Similar to individual models, it achieves optimal accuracy in the higher range.

Size. Figure 5 presents the accuracy achieved by our model at inference time with respect to the number of residual blocks (and size) of the trained restoration network. With only two residual blocks, our model achieves 98.6% of the optimal PSNR. Using four residual blocks, our model obtains slightly better accuracy than the current state-of-the-art model [11], using only $\sim \frac{1}{2.26}$ of the parameters. This

Table 4: Accuracy outside the trained range. The results are for image denoising.

	PSNR (dB)				
	5	10	80	85	90
Baseline	40.48	36.35	26.21	25.95	25.74
DNI	23.64	29.52	25.26	23.01	20.30
AdaFM	38.80	36.16	26.03	25.61	24.76
DeCoupling	34.40	32.9	20.94	20.72	20.49
CFSnet	29.43	29.3	25.79	25.55	25.31
Ours	39.96	36.22	26.21	25.95	25.71
Distance (Ours)	0.52	0.13	0.00	0.00	0.02

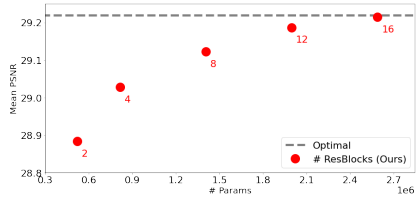


Figure 5: Accuracy of our model with respect to the number of residual blocks in the restoration network. The dashed gray line is the optimal average accuracy, obtained by training multiple dedicated models. The red dots are the number of residual blocks.

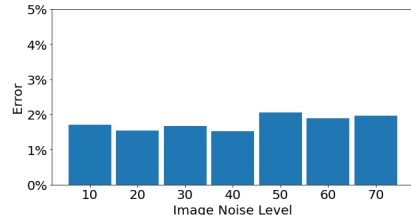


Figure 6: Noise level estimation. Our simple CNN model estimates the ground truth noise level with an error rate of 1.77%. See text for more details.

implies that optimizing the weights of multiple networks simultaneously can improve the model’s generalization. Using all sixteen residual blocks, our approach can achieve state-of-the-art accuracy.

Blind Image Restoration. A continuous image restoration model is designed to provide the user with the ability to adjust the restoration output at runtime. In order to provide the restoration output corresponding to the input degradation level when the level is unknown, we train a simple CNN (five convolutional layers and three fully connected layers) to estimate the degradation level of a noisy image. Based on our trained network, we can estimate the input degradation level and set the encoding scalar \bar{c}_i accordingly. Fig. 6 and 7 demonstrate the accuracy of the noise estimation network. Fig. 6 shows the error of the estimation as a

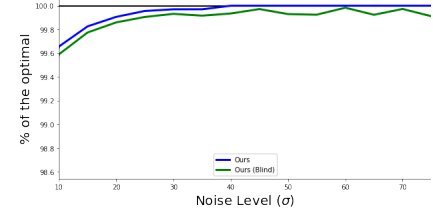


Figure 7: Blind restoration. Using our noise level estimator, our model can accurately denoise the input images for all the ranges.

percentage of the ground truth noise level. On average, the degradation level estimation network achieves an accuracy of 98.23%. Fig. 7, obtained by setting the input degradation level for each degraded image according to the estimated degradation level, shows the effect of the estimated degradation level on the final restoration accuracy of our model. Overall, the estimation of noise level results in accurate restoration and can be advantageous in cases where the actual degradation level is unknown.

Degradation Parameter Accuracy We experiment with the ability of the hypernetwork at inference time to generate, as trained, the optimal weights for the corresponding input degradation level. For each image in the test set, we degrade the image with a specific degradation level, e.g. $\sigma = 15$ for the denoising task. For the degraded image, we measure the best input parameter that yields the network with the highest restoration accuracy in terms of PSNR. Fig. 8 presents both the ground truth degradation level and the best input degradation level with respect to different levels for the denoising (top) and DeJPEG (bottom) tasks. As can be seen, our approach achieves a high level of restoration quality by generating weights according to the input degradation level. Similar results were obtained for super-resolution. Figure 10 shows the result of adjusting our model, for the DeJPEG task. The restoration effect is according to the input degradation level, as required.

4.4. Ablation Study

Batch Normalization and Bias. We explore the optimal architecture of our default main restoration network with respect to bias and batch normalization (BN) [15]. For batch normalization testing, we train a network with BNs after all convolutional layers and adjust the statistics in BN layers during testing. The results are shown in Table 5. It can be seen that bias is an essential ingredient in our approach. Using batch normalization without bias does not result in a successful restoration. Batch normalization used with bias produces comparable results to bias-only in the range of 15–75. We deploy the bias-only configuration as our default one due to its simplicity.

Number of Main Networks. We explore the number of

Table 5: The architecture of our model with and without bias and batch normalization. We use the 4 main networks, $\sigma = 15, 35, 50, 75$, as the baseline.

		PSNR (dB)								
		5	15	25	35	45	55	65	75	85
Baseline		40.48	34.08	31.42	29.80	28.64	27.78	27.06	26.46	25.95
With BN		34.50	33.97	31.35	29.76	28.61	27.73	27.01	26.43	22.38
With Bias		39.96	34.02	31.41	29.80	28.64	27.78	27.06	26.46	25.95
BN and Bias		35.46	33.98	31.30	29.77	28.61	27.73	27.00	26.44	23.20

Table 6: Our 16-layers approach trained to restore 5 noise levels vs. 32-layer adaptive CResMD

		PSNR (dB)								
		5	15	25	35	45	55	65	75	85
Baseline		40.48	34.08	31.42	29.80	28.64	27.78	27.06	26.46	25.95
CResMD		40.15	33.93	31.30	29.67	28.52	27.63	26.89	26.23	25.60
Ours (5)		40.31	34.00	31.39	29.78	28.64	27.77	27.06	26.46	25.95

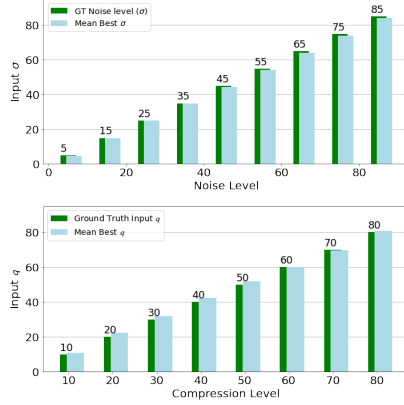


Figure 8: Parameter accuracy. The dark green bars represent the ground truth degradation levels (the numbers above) while the light green bars represent the mean value of the best input parameter that achieves the highest restoration accuracy. The top row is denoising and the bottom row is DeJPEG.

main networks in the model and their effect on the performance. We experiment with various configurations for our model, from one to five different main networks. Note that the number of main networks does not change the final size of our model at inference, only at training.

For the denoising task, for the model with two networks we use $\sigma = 1[5, 75]$. For the model with three main networks we use $\sigma = [15, 45, 85]$. For the model with four main networks we use $\sigma = [15, 35, 50, 75]$ and for the model with five main networks we use $\sigma = [5, 25, 45, 65, 85]$. Table 7 presents the PNSR obtained by each model. For the range of 15–85, the model trained with four main networks is comparable to the model trained with five main networks. For noise level 5, the model trained with five main networks obtained higher accuracy. We fur-

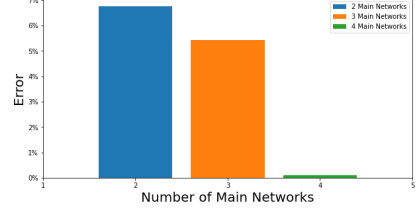


Figure 9: The effect of the number of main networks for super-resolution. The x-axis is the number of objectives our model is trained to adapt. The y-axis is the average error in percentages relative to multiple optimal models trained to restore the correspondent upscaling. Our model can achieve optimal accuracy by increasing the number of main networks to four.

ther explore the performance of our approach with four and five main networks with respect to continuous restoration networks with a higher number of layers. We report results for CResMD [10] which includes almost twice as many layers (32) as our network. Although CResMD learns multiple types of degradation, it has been shown to outperform state-of-the-art methods for continuous denoising. Table 6 shows the results of our approach and CResMD for the denoising task. Overall, CResMD is better than both AdaFM and DNI and our approach outperforms all three. It can be seen that the four and five networks' models perform similarly apart from the lowest noise level. This suggests that for obtaining higher accuracy along with a wider range, one might need to train a model with a sufficient number of main networks.

For super-resolution we experiment with the following ranges: $[\times 2, \times 4]$, $[\times 2, \times 3, \times 4]$ and $[\times 2, \times 3, \times 4, \times 5]$. Figure 9 shows the results for the super-resolution task. Overall, the results indicate that by increasing the number of main networks to four, the accuracy is significantly im-

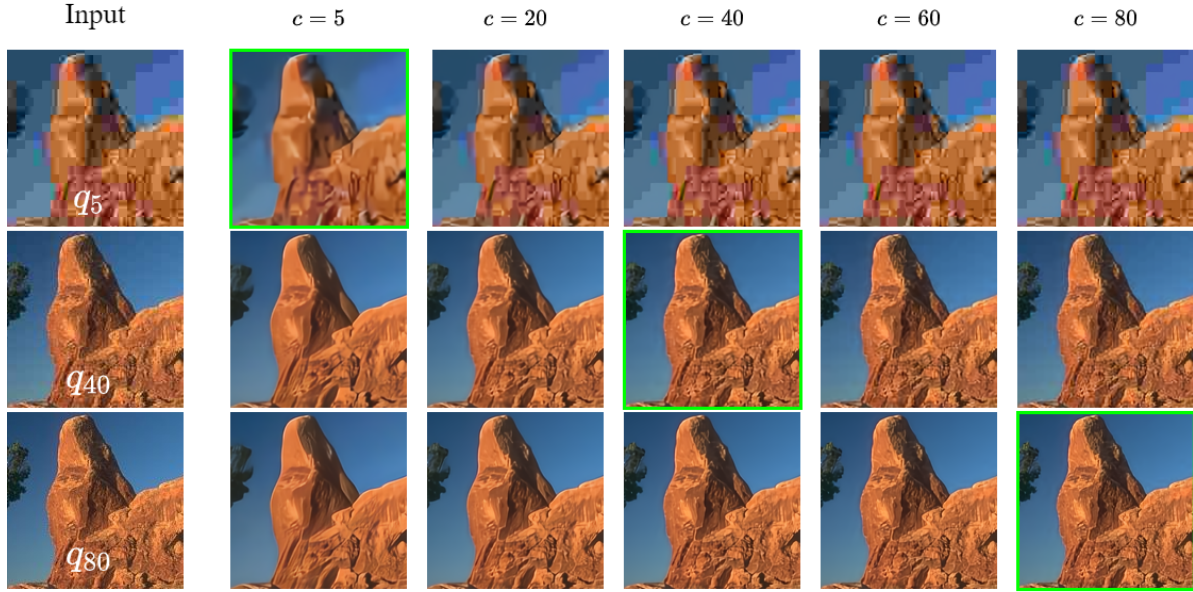


Figure 10: The result of applying our model for various compressed images. Each compressed image was restored using different JPEG compression levels. The best restoration was achieved when the network was fed with the same compression degree as the input image.

Table 7: The results for our image denoising models, each is trained with a different number of main networks.

	PSNR (dB)								
	5	15	25	35	45	55	65	75	85
Baseline	40.48	34.08	31.42	29.80	28.64	27.78	27.06	26.46	25.95
2 main networks	36.46	34.02	29.94	27.66	26.95	26.89	26.82	26.46	25.12
3 main networks	39.55	34.02	31.39	29.78	28.64	27.77	27.06	26.46	25.94
4 main networks	39.96	34.02	31.41	29.80	28.64	27.78	27.06	26.46	25.95
5 main networks	40.31	34.00	31.39	29.78	28.64	27.77	27.06	26.46	25.95

proved. Due to the fact that at inference time we deploy a fixed-size single model regardless of the number of main networks trained, adding more main networks is beneficial.

We also experiment with DeJPEG on three different models ($q = [10, 40, 80]$, $q = [10, 30, 50, 80]$ and $q = [10, 25, 45, 65, 80]$). The results are similar as to previous tasks, the accuracy of restoration increases with the number of main networks.

5. Conclusion

The task of real-world image restoration is challenging since the exact input degradation level and the user’s preferences for the restoration effect are unknown. Current approaches compromise either accuracy, the range of the degradation levels they support, or the size of the model. The combination of all three is imperative for a fully functional real-world solution, but such a method is currently unavailable. We introduce a hypernetwork for continuous

image restoration that is accurate, maintains a small footprint during inference and can support a wide range of degradation levels. It is capable of efficiently generating the weights of a restoration network to best adapt to a given level of degradation. Our approach outperforms state-of-the-art methods in this very competitive field, for both denoising, DeJPEG, and super-resolution tasks.

References

- [1] Eirikur Agustsson and Radu Timofte. Ntire 2017 challenge on single image super-resolution: Dataset and study. In *The IEEE Conference on Computer Vision and Pattern Recognition (CVPR) Workshops*, July 2017.
- [2] Marco Bevilacqua, Aline Roumy, Christine Guillemot, and Marie line Alberi Morel. Low-complexity single-image super-resolution based on nonnegative neighbor embedding. In *Proceedings of the British Machine Vision Conference*, pages 135.1–135.10. BMVA Press, 2012.

[3] G. Bradski. The OpenCV Library. *Dr. Dobb's Journal of Software Tools*, 2000.

[4] Andrew Brock, Theodore Lim, J. M. Ritchie, and Nick Weston. Smash: One-shot model architecture search through hypernetworks, 2017.

[5] Chao Dong, Yubin Deng, Chen Change Loy, and Xiaoou Tang. Compression artifacts reduction by a deep convolutional network, 2015.

[6] Noam Elron, Shahar S. Yuval, Dmitry Rudoy, and Noam Levy. Blind image restoration without prior knowledge, 2020.

[7] Thomas Elsken, Jan Hendrik Metzen, and Frank Hutter. Neural architecture search: A survey. *The Journal of Machine Learning Research*, 20(1):1997–2017, 2019.

[8] Qingnan Fan, Dongdong Chen, Lu Yuan, Gang Hua, Nenghai Yu, and Baoquan Chen. Decouple learning for parameterized image operators. In *Proceedings of the European Conference on Computer Vision (ECCV)*, pages 442–458, 2018.

[9] David Ha, Andrew Dai, and Quoc V. Le. Hypernetworks, 2016.

[10] Jingwen He, Chao Dong, and Yu Qiao. Interactive multi-dimension modulation with dynamic controllable residual learning for image restoration. *arXiv preprint arXiv:1912.05293*, 2019.

[11] Jingwen He, Chao Dong, and Yu Qiao. Modulating image restoration with continual levels via adaptive feature modification layers. In *The IEEE Conference on Computer Vision and Pattern Recognition (CVPR)*, June 2019.

[12] Kaiming He, Xiangyu Zhang, Shaoqing Ren, and Jian Sun. Deep residual learning for image recognition. In *Proceedings of the IEEE conference on computer vision and pattern recognition*, pages 770–778, 2016.

[13] A. Horé and D. Ziou. Image quality metrics: Psnr vs. ssim. In *2010 20th International Conference on Pattern Recognition*, pages 2366–2369, 2010.

[14] Xuecai Hu, Haoyuan Mu, Xiangyu Zhang, Zilei Wang, Tieniu Tan, and Jian Sun. Meta-sr: A magnification-arbitrary network for super-resolution. In *Proceedings of the IEEE/CVF conference on computer vision and pattern recognition*, pages 1575–1584, 2019.

[15] Sergey Ioffe and Christian Szegedy. Batch normalization: Accelerating deep network training by reducing internal covariate shift, 2015.

[16] Wei Jiang, Wei Wang, Shan Liu, and Songnan Li. Png: Micro-structured prune-and-grow networks for flexible image restoration. In *Proceedings of the IEEE/CVF Conference on Computer Vision and Pattern Recognition*, pages 756–765, 2021.

[17] Amlan Kar, Aayush Prakash, Ming-Yu Liu, Eric Cameracci, Justin Yuan, Matt Rusiniak, David Acuna, Antonio Torralba, and Sanja Fidler. Meta-sim: Learning to generate synthetic datasets. In *Proceedings of the IEEE/CVF International Conference on Computer Vision*, pages 4551–4560, 2019.

[18] David Krueger, Chin-Wei Huang, Riashat Islam, Ryan Turner, Alexandre Lacoste, and Aaron Courville. Bayesian hypernetworks. *arXiv preprint arXiv:1710.04759*, 2017.

[19] Hyeongmin Lee, Taeoh Kim, Hanbin Son, Sangwook Baek, Minsu Cheon, and Sangyoun Lee. Smoother network tuning and interpolation for continuous-level image processing. *arXiv preprint arXiv:2010.02270*, 2020.

[20] Bee Lim, Sanghyun Son, Heewon Kim, Seungjun Nah, and Kyoung Mu Lee. Enhanced deep residual networks for single image super-resolution. In *Proceedings of the IEEE conference on computer vision and pattern recognition workshops*, pages 136–144, 2017.

[21] Benlin Liu, Yongming Rao, Jiwen Lu, Jie Zhou, and Chou-Jui Hsieh. Metadistiller: Network self-boosting via meta-learned top-down distillation. In *European Conference on Computer Vision*, pages 694–709. Springer, 2020.

[22] David Martin, Charless Fowlkes, Doron Tal, and Jitendra Malik. A database of human segmented natural images and its application to evaluating segmentation algorithms and measuring ecological statistics. In *Proceedings Eighth IEEE International Conference on Computer Vision. ICCV 2001*, volume 2, pages 416–423. IEEE, 2001.

[23] Adam Paszke, Sam Gross, Francisco Massa, Adam Lerer, James Bradbury, Gregory Chanan, Trevor Killeen, Zeming Lin, Natalia Gimelshein, Luca Antiga, Alban Desmaison, Andreas Kopf, Edward Yang, Zachary DeVito, Martin Raison, Alykhan Tejani, Sasank Chilamkurthy, Benoit Steiner, Lu Fang, Junjie Bai, and Soumith Chintala. Pytorch: An imperative style, high-performance deep learning library. In H. Wallach, H. Larochelle, A. Beygelzimer, F. d'Alché-Buc, E. Fox, and R. Garnett, editors, *Advances in Neural Information Processing Systems 32*, pages 8024–8035. Curran Associates, Inc., 2019.

[24] Pengzhen Ren, Yun Xiao, Xiaojun Chang, Po-Yao Huang, Zhihui Li, Xiaojiang Chen, and Xin Wang. A comprehensive survey of neural architecture search: Challenges and solutions. *arXiv preprint arXiv:2006.02903*, 2020.

[25] Abdul-Saboor Sheikh, Kashif Rasul, Andreas Merentitis, and Urs Bergmann. Stochastic maximum likelihood optimization via hypernetworks. *arXiv preprint arXiv:1712.01141*, 2017.

[26] H. R. Sheikh, M. F. Sabir, and A. C. Bovik. A statistical evaluation of recent full reference image quality assessment algorithms. *IEEE Transactions on Image Processing*, 15(11):3440–3451, 2006.

[27] Falong Shen, Shuicheng Yan, and Gang Zeng. Neural style transfer via meta networks. In *Proceedings of the IEEE Conference on Computer Vision and Pattern Recognition*, pages 8061–8069, 2018.

[28] Wenzhe Shi, Jose Caballero, Ferenc Huszár, Johannes Totz, Andrew P Aitken, Rob Bishop, Daniel Rueckert, and Zehan Wang. Real-time single image and video super-resolution using an efficient sub-pixel convolutional neural network. In *Proceedings of the IEEE conference on computer vision and pattern recognition*, pages 1874–1883, 2016.

[29] Wenzhe Shi, Jose Caballero, Ferenc Huszár, Johannes Totz, Andrew P Aitken, Rob Bishop, Daniel Rueckert, and Zehan Wang. Real-time single image and video super-resolution using an efficient sub-pixel convolutional neural network. In *Proceedings of the IEEE conference on computer vision and pattern recognition*, pages 1874–1883, 2016.

- [30] Alon Shoshan, Roey Mechrez, and Lihi Zelnik-Manor. Dynamic-net: Tuning the objective without re-training for synthesis tasks. In *The IEEE International Conference on Computer Vision (ICCV)*, October 2019.
- [31] Wei Wang, Ruiming Guo, Yapeng Tian, and Wenming Yang. Cfsnet: Toward a controllable feature space for image restoration, 2019.
- [32] Xintao Wang, Ke Yu, Chao Dong, Xiaoou Tang, and Chen Change Loy. Deep network interpolation for continuous imagery effect transition, 2018.
- [33] Zhihao Wang, Jian Chen, and Steven CH Hoi. Deep learning for image super-resolution: A survey. *IEEE transactions on pattern analysis and machine intelligence*, 43(10):3365–3387, 2020.
- [34] Junyuan Xie, Linli Xu, and Enhong Chen. Image denoising and inpainting with deep neural networks. *Advances in neural information processing systems*, 25:341–349, 2012.
- [35] Zhou Yu, Yuhao Cui, Jun Yu, Meng Wang, Dacheng Tao, and Qi Tian. Deep multimodal neural architecture search. In *Proceedings of the 28th ACM International Conference on Multimedia*, pages 3743–3752, 2020.
- [36] Kai Zhang, Wangmeng Zuo, Yunjin Chen, Deyu Meng, and Lei Zhang. Beyond a gaussian denoiser: Residual learning of deep CNN for image denoising. *IEEE Transactions on Image Processing*, 26(7):3142–3155, jul 2017.
- [37] Yulun Zhang, Yapeng Tian, Yu Kong, Bineng Zhong, and Yun Fu. Residual dense network for image restoration, 2018.
- [38] Yulun Zhang, Yapeng Tian, Yu Kong, Bineng Zhong, and Yun Fu. Residual dense network for image super-resolution. In *Proceedings of the IEEE conference on computer vision and pattern recognition*, pages 2472–2481, 2018.
- [39] H. Zhao, O. Gallo, I. Frosio, and J. Kautz. Loss functions for image restoration with neural networks. *IEEE Transactions on Computational Imaging*, 3(1):47–57, 2017.